Earthquake Engineering & Structural Dynamics
The Journal of the International Association for Earthquake Engineering

EARTHQUAKE ENGINEERING & STRUCTURAL DYNAMICS
Earthquake Engng Struct. Dyn. **2012**
Published online in Wiley Online Library (wileyonlinelibrary.com). DOI: 10.1002/eqe.2209

Response of base-isolated nuclear structures for design and beyond-design basis earthquake shaking

Yin-Nan Huang[1,*,†], Andrew S. Whittaker[2], Robert P. Kennedy[3] and Ronald L. Mayes[4]

[1]*Department of Civil Engineering, National Taiwan University, No. 1, Sec. 4, Roosevelt Road, Taipei, 10617, Taiwan*
[2]*Department of Civil, Structural and Environmental Engineering, University at Buffalo, State University of New York, Buffalo, NY 14260, USA*
[3]*RPK Structural Mechanics Consulting Inc., Escondido, CA 92026, USA*
[4]*Simpson Gumpertz & Heger Inc., San Francisco, CA 94105, USA*

SUMMARY

The American Society of Civil Engineers (ASCE) 43-05 presents two performance objectives for the design of nuclear structures, systems and components in nuclear facilities: (1) 1% probability of unacceptable performance for 100% design basis earthquake (DBE) shaking and (2) 10% probability of unacceptable performance for 150% DBE shaking. To aid in the revision of the ASCE 4-98 procedures for the analysis and design of base-isolated nuclear power plants and meet the intent of ASCE 43-05, a series of nonlinear response-history analyses was performed to study the impact of the variability in both earthquake ground motion and mechanical properties of isolation systems on the seismic responses of base-isolated nuclear power plants. Computations were performed for three representative sites (rock and soil sites in the Central and Eastern United States and a rock site in the Western United States) and three types of isolators (lead rubber, Friction Pendulum and low-damping rubber bearings) using realistic mechanical properties for the isolators. Estimates were made of (1) the ratio of the 99th percentile (90th percentile) response of isolation systems computed using a distribution of spectral demands and distributions of isolator mechanical properties to the median response of isolation systems computed using best-estimate properties and 100% (150%) spectrum-compatible DBE ground motions; (2) the number of sets of three-component ground motions to be used for response-history analysis to develop a reliable estimate of the median response of isolation systems. The results of this study provide the technical basis for the revision of ASCE Standard 4-98. Copyright © 2012 John Wiley & Sons, Ltd.

Received 20 February 2012; Revised 24 April 2012; Accepted 1 May 2012

KEY WORDS: **nuclear power plant; base isolation; design basis earthquake; rubber bearing; Friction Pendulum**

1. INTRODUCTION

Base isolation has been used to protect buildings, bridges and mission-critical infrastructure from the damaging effects of earthquake shaking [1, 2]. It has been implemented in safety-related nuclear structures in France and South Africa [3]. In the United States, there are no applications of seismic isolation to nuclear structures at the time of this writing although some vendors of Nuclear Steam Supply Systems and power utilities are considering seismic isolation for new build plants.

Seismic isolation systems worthy of consideration for application to nuclear facilities in North America include two types of elastomeric bearings and one type of sliding bearing. Lead–rubber (LR) and low-damping rubber (LDR) bearings are examples of elastomeric bearings. The sliding bearing that is suitable for application to nuclear structures is the Friction Pendulum (FP) (Earthquake Protection

***Correspondence to: Yin-Nan Huang, Department of Civil Engineering, National Taiwan University, Taiwan; Address: No. 1, Sec. 4, Roosevelt Road, Taipei, 10617 Taiwan.**
†E-mail: ynhuang@ntu.edu.tw

Systems, Inc., Vallejo, California) bearing. These elastomeric and sliding seismic isolation bearings are stiff in the vertical direction and flexible in any horizontal direction. The horizontal flexibility of the isolation system increases the fundamental period of the supported structure and reduces the inertial forces in the supported structure, enabling the secondary systems to be designed for much smaller forces and displacements than in a conventional (nonisolated) structure. Naeim and Kelly [4] and Constantinou *et al*. [5] provided much information on seismic isolation and isolators. Huang *et al*. [6–8] identified the benefits of seismic isolation for nuclear structures using risk-based approaches that are consistent with US nuclear practice.

Two American Society of Civil Engineers (ASCE) standards are relevant to the analysis and design of nuclear power plants (NPPs): ASCE 4-98, *Seismic Analysis of Safety-Related Nuclear Structures and Commentary* [9] and ASCE 43-05, *Seismic Design Criteria for Structures, Systems and Components in Nuclear Facilities* [10]. Section 1.3 of ASCE 43-05 presents dual performance objectives for nuclear structures, systems and components (SSCs): (1) 1% probability of unacceptable performance for 100% design basis earthquake (DBE) shaking and (2) 10% probability of unacceptable performance for 150% DBE shaking. The dual performance objectives were established to achieve a mean annual frequency of exceedance (MAFE) less than 10^{-5} for the first onset of significant inelastic deformation of safety-related SSCs in nuclear facilities [10]. ASCE Standard 4-98, which includes rudimentary provisions for the analysis and design of seismic isolation systems, is being revised at this time and the studies reported in this paper provide the technical basis for the proposed changes, which will satisfy the risk-informed goals of ASCE 43-05.

In base-isolated nuclear structures, the accelerations and deformations in SSCs are relatively small. As such, unacceptable performance of an isolated nuclear structure subjected to both DBE shaking and beyond design basis shaking will most likely involve either the failure of isolation bearings or impact of the isolated superstructure and surrounding buildings or geotechnical structures. Three performance statements for achieving the above two performance objectives of ASCE 43-05 were used for the studies presented herein, namely (1) individual isolators shall suffer no damage in DBE shaking, (2) the probability of the isolated nuclear structure impacting surrounding structure (moat) for 100% (150%) DBE shaking is 1% (10%) or less, and (3) individual isolators sustain gravity and earthquake-induced axial loads at 90th percentile lateral displacements consistent with 150% DBE shaking. Performance statements 1 and 3 can be realized by testing isolators and statement 2 can be supported using analysis in which (a) the ground motion representations are reasonable and (b) the isolators are modeled properly.

The state-of-practice in selecting and scaling ground motions for design of conventional and isolated buildings and nuclear infrastructure involves selecting pairs of earthquake ground motions on the basis of earthquake magnitude, site-to-source distance and local soil conditions and scaling these motions to a design spectrum so that the resultant motions are spectrum-compatible. Although straightforward, such scaling cannot capture the distribution of spectral demand around the geometric mean demand, which is typically the product of a seismic hazard assessment. Alternate scaling procedures are used in this study to assess the performance of isolated nuclear structures.

The mechanical properties of typical seismic isolators such as LDR, LR, and FP bearings will tend to vary from the values assumed for design both (a) at the time of fabrication because of variability in basic material properties and (b) over the lifespan of the nuclear structure because of aging, contamination, ambient temperature, etc. The mechanical properties of LDR bearings are a function of the raw materials used, the choice of rubber compound and the thermal and pressure profiles used to cure the bearings. For LR bearings, the mechanical properties of the lead plug are a function of the confinement provided to the plug and the mechanical properties of the elastomer (rubber). For FP bearings, only the coefficient of sliding friction varies because the second-slope stiffness of the bearing is a function of the radius of the sliding surface, which is constructed to very tight tolerances. Importantly, the variability of the mechanical properties of an assembly of isolators (the isolation system) will be smaller than the variability of individual isolators. The state-of-practice of seismic isolation system analysis and design is to develop lower and upper bound properties for the isolation system using property modification factors [5, 11–13], to use the best-estimate, lower-bound, and upper-bound mechanical properties for analysis, and then envelope the resultant displacements and transmitted forces for design and assessment. The basic force–displacement relationship used to analyze LR and FP bearing isolation systems is shown in Figure 1. This model is fully defined by a characteristic strength,

DOI: 10.1002/eqe

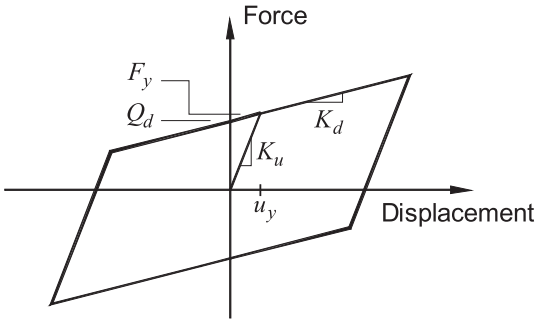

Figure 1. A force–displacement relationship similar to that used in the analysis for this study for the LR and FP bearings in the horizontal directions.

Q_d, and a second-slope (post-yield) stiffness, K_d. The second-slope stiffness is related to the isolated period through the supported weight, W. Low-damping rubber bearings are modeled typically as linearly elastic elements with displacement-independent damping.

In the studies presented in this paper, we performed a series of nonlinear response-history analyses accounting for the variability in both earthquake ground motion and the mechanical properties of isolation systems. The goals of the studies were three-fold, namely (1) determine the ratio of the 99th percentile estimate of the displacement (force) computed using a distribution of DBE spectral demands and distributions of isolator mechanical properties to the median isolator displacement (force) computed using best-estimate properties and spectrum-compatible DBE shaking; (2) determine the ratio of the 90th percentile estimate of the displacement (force) computed using a distribution of 150% DBE spectral demands and distributions of isolator mechanical properties to the median isolator displacement (force) computed using best-estimate properties and spectrum-compatible DBE shaking, and (3) determine the number of sets of three-component ground motions to be used for response-history analysis to develop a reliable estimate of the median displacement (force).

Computations were performed for representative rock and soil sites in the Central and Eastern United States (CEUS) and a rock site in the Western United States (WUS). Three types of isolators, namely, low-damping rubber, lead–rubber and Friction Pendulum bearings, and realistic mechanical properties for the isolators were used in the analysis. Section 2 introduces the base-isolation systems and numerical models analyzed in this study. Sections 3, 4, and 5 present the analyses for the sample CEUS rock, CEUS soil, and WUS rock sites, respectively. Each of Sections 3, 4, and 5 includes information for DBE shaking, selection, and scaling of ground motions, analysis procedure and results. Section 6 summarizes the results of Sections 3, 4, and 5 and provides recommendations on the analysis procedures for the seismic design of base-isolated nuclear structures.

The analyses presented in this paper do not address torsional response of isolated nuclear structures. If the increment in displacement response due to torsion is a significant percentage of the displacement at the center of mass of the isolated superstructure, the conclusions and recommendations presented below must be used with care. Furthermore, the change in isolator mechanical properties over the course of earthquake shaking was not addressed in the studies presented herein.

2. BASE ISOLATION SYSTEMS

2.1. Models of isolation systems

SAP2000 Nonlinear [14] was used to perform the response-history analysis of models of base-isolated NPPs. Each model was composed of a rigid mass supported by a link element representing the isolation system. Each model had three degrees of freedom: two horizontal and one vertical. The models for each type of the isolation system used in the analysis are described below:

Lead–rubber isolation systems were modeled using the 'Rubber Isolator' link element in SAP2000. This element has coupled plasticity properties for the two horizontal displacements and linear stiffness properties for the vertical displacement. The plasticity model is similar to that of Figure 1 but the

DOI: 10.1002/eqe

transition between the elastic stiffness and the post-yield stiffness is continuous. To study a wide range of isolation-system properties, nine best-estimate models were prepared with characteristic strength Q_d equal to 3%, 6% and 9% of the supported weight W, and T_d (the period related to the post-yield stiffness of the isolator K_d through W) equal to 2, 3, and 4 s. Parameter T_v (the period related to the vertical stiffness of the isolation system K_v through W) was set to 0.05 s. The models are termed LR_TxQy, where x denotes the value of T_d and y denotes the percentage of Q_d/W. For example, the model of LR_T2Q3 has a T_d of 2 s and Q_d/W of 3%. Because the intensity and frequency content of DBE shaking for the three sites studied herein are significantly different, the mechanical properties of base isolation systems appropriate for each site are not identical. For example, an isolation system with $Q_d = 0.09W$ is considered unrealistic for rock sites in the CEUS, where the DBE shaking is generally much smaller than $0.1g$ at periods greater than 2 s. Only results for realistic isolation systems at a given site are presented in this paper.

Friction Pendulum isolators were modeled using the 'Friction Isolator' link element that has coupled plasticity properties for the two horizontal directions and a gap element for vertical tensile forces. The coefficient of friction for FP bearings depends on the sliding velocity and is computed in SAP2000 using the following equation [11]:

$$\mu = \mu_{max} - (\mu_{max} - \mu_{min}) \cdot e^{-aV} \tag{1}$$

where μ is the coefficient of sliding friction, varying between μ_{max} and μ_{min} (for high and very small velocities, respectively), a is a velocity-related parameter, and V is the sliding velocity. A value of a= 55 s/m was adopted for this study based on the experimental data of Fenz and Constantinou [15]. The hysteresis loop for the FP bearings will collapse to the bilinear loop of Figure 1 for Coulomb friction (i.e., $a = \infty$) with $Q_d = \mu_{max} W$. Nine best-estimate FP isolation-system models were analyzed in this study with μ_{max} equal to 0.03, 0.06 and 0.09 and T_d equal to 2, 3, and 4 s but only the results for realistic models at a given site are presented. The yield displacement was set at 1 mm for all FP models. The models are termed FP_TxQy, where the definitions of x and y are the same as those for LR isolators.

Low-damping rubber isolators were modeled in SAP2000 using the 'Linear' link element where the elastic stiffness and damping can be assigned in each degree of freedom. Three best-estimate models were studied with T_h (the period related to the horizontal elastic stiffness of the isolator K_h through W) equal to 2, 3, and 4 s, and T_v equal to 0.05 s. Three-percent damping was assigned to the two horizontal degrees of freedom of the isolation systems. The three models are termed LDR_T2, LDR_T3 and LDR_T4 for T_h equal to 2, 3, and 4 s, respectively. The analyses using LDR isolators are performed for the sample rock site in the CEUS only because the DBE shaking for this site has very small seismic demands in the long period range, even for lightly-damped systems (see Figure 4).

It must be noted that the force–displacement relationships described above do not represent all possible LDR, LR, and FP isolators. At very high shearing strains in LDR and LR isolators, the elastomer will stiffen (harden), which will produce a trilinear force–displacement relationship. This relationship is difficult to model a priori because the strain at the onset of stiffening is a function of the chosen rubber compound. (Because isolators should be analyzable for design and beyond design basis shaking, shearing strains should be limited to values smaller than the strain at the onset of stiffening.) The chosen models are appropriate for the single concave FP bearing. The recently developed triple concave FP bearing [15] can be configured to provide a horizontal force–displacement relationship similar to that of the LR bearing.

2.2. Variations in properties of isolators

To study the impact of variations in mechanical properties of isolators on the response of base-isolated NPPs, two sets of 30 mathematical models were developed for each of the best-estimate models studied herein by modifying the values of key parameters of the best-estimate models. For LR models, Q_d, K_d and K_v were assumed to vary; for FP models, only μ_{max} was assumed to vary; and for LDR models, K_h and K_v were assumed to vary. One set of 30 models represents an isolation *system* with *excellent*

DOI: 10.1002/eqe

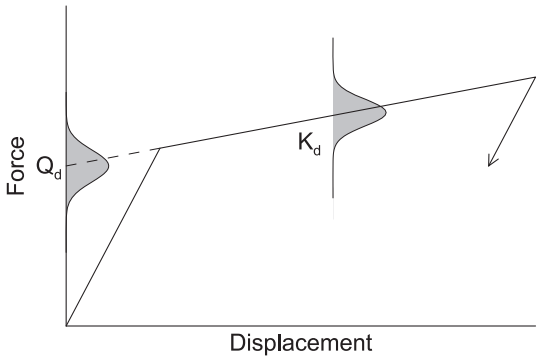

Figure 2. Variations in the mechanical properties of a LR isolation system.

control on the properties of individual isolators: the probability for the values of the key parameters of the isolation system described above to be within $\pm$10% of the best-estimate values is 95% (Bin F1). The second set represents an isolation system with good control on the properties of individual isolators: the probability for the values of the key parameters of the isolation system to be within $\pm$20% of the best-estimate values is 95% (Bin F2). We assume the distributions for the values of the key parameters to be normal. As an example, Figure 2 illustrates these distributions in parameters Q_d and K_d for LR isolation systems. Bins F1 and F2 likely address the permissible ranges of mechanical properties of an isolation system[1] for NPP construction. An isolation system with a greater variation in mechanical properties than that associated with Bin F2 should not be used for NPPs.

To develop the two sets of 30 mathematical models, two bins of 30 scale factors were generated, where the factors for Bin F1 (F2) were obtained from a normal distribution with a mean of 1 and a standard deviation of 0.05 (0.1). Figure 3 presents the two normal distributions. For each of these curves in Figure 3, the area under the curve was divided into 30 equal segments; the midpoint value in each segment is reported in Table I and used to form the factors for Bins F1 and F2.

The generation of the two sets of 30 models for each best-estimate LR model is described herein to demonstrate the process. For each best-estimate LR model, the values of Q_d, K_d and K_v were scaled by two sets of factors: [$F1_i^{Q_d}$, $F1_i^{K_d}$, $F1_i^{K_v}$] and [$F2_i^{Q_d}$, $F2_i^{K_d}$, $F2_i^{K_v}$], where $F1_i^{Q_d}$, $F1_i^{K_d}$, and $F1_i^{K_v}$ ($F2_i^{Q_d}$, $F2_i^{K_d}$, and $F2_i^{K_v}$) are the scale factors for Q_d, K_d, and K_v, respectively, determined from the 30 scale factors in Bin F1 (F2) using the Latin Hypercube Sampling procedure [16] and i= 1 through 30. For each value of i, a new model (i.e., a new combination of Q_d, K_d, and K_v) was developed for each case of excellent and good control.

The procedures described above were repeated for the FP and LDR isolation systems. The developed models were used in the response-history analysis to study the impact of variations in material properties of isolators on the response of base-isolated NPPs.

3. STUDIES FOR A ROCK SITE IN CEUS

3.1. Ground motions

3.1.1. Design basis earthquake. The North Anna NPP site in Louisa County, VA is a representative rock site for NPPs in CEUS. The horizontal and vertical DBE spectra used in this study for the North Anna site are presented in Figure 4. The horizontal spectrum of Figure 4 is a uniform-risk spectrum corresponding to a MAFE of 10^{-5} based on the data presented in an Early Site Permit Application report for North Anna [17]. The horizontal DBE spectrum of Figure 4 was scaled by the V/H factors recommended by Bozorgnia and Campbell [18] to generate the vertical DBE spectrum.

[1]Given that an isolation system consists of a large number of isolators, larger percentage variations in the mechanical properties of individual isolators might be acceptable.

DOI: 10.1002/eqe

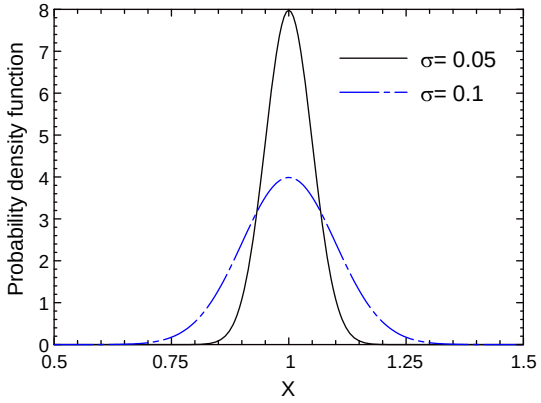

Figure 3. Normal distributions with a mean of 1 and standard deviations of 0.05 and 0.1.

Table I. Scale factors for mechanical properties of bearings.

Bin	Scale factors
F1	0.894, 0.918, 0.931, 0.940, 0.948, 0.955, 0.961, 0.966, 0.971, 0.976, 0.981, 0.985, 0.990, 0.994, 0.998, 1.002, 1.006, 1.011, 1.015, 1.019, 1.024, 1.029, 1.034, 1.039, 1.045, 1.052, 1.060, 1.069, 1.082, 1.106
F2	0.787, 0.836, 0.862, 0.881, 0.896, 0.910, 0.922, 0.933, 0.943, 0.952, 0.962, 0.970, 0.979, 0.987, 0.996, 1.004, 1.013, 1.021, 1.030, 1.039, 1.048, 1.057, 1.067, 1.078, 1.090, 1.104, 1.119, 1.138, 1.165, 1.213

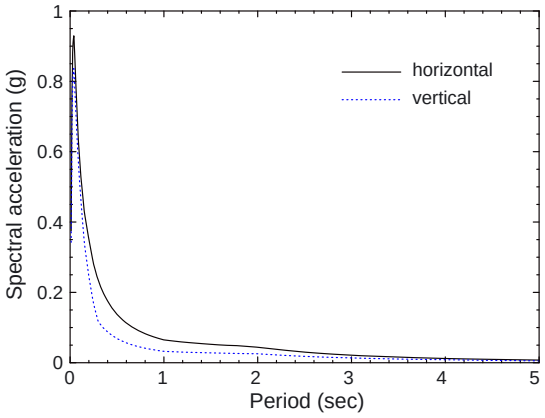

Figure 4. Horizontal and vertical 5% damped DBE spectra for the North Anna NPP site.

3.1.2. DBE spectrum-compatible ground motions. **Two bins of 30 sets of ground motions were developed for the response-history analysis to study the impact of the variability in earthquake ground motion on the response of base-isolated NPPs. In the first bin, termed DBE spectrum-compatible (DBE-SC) ground motions, both of the two horizontal components of each set of ground motions have 5% damped spectral accelerations similar to that of Figure 4. In the second bin, termed maximum–minimum spectrum-compatible (MM-SC) ground motions, the variability in spectral acceleration along three perpendicular directions is addressed in the scaling of ground motions. The development of these two bins of ground motions are summarized in this and the following subsections, respectively. More information can be found in [19].**

DOI: 10.1002/eqe

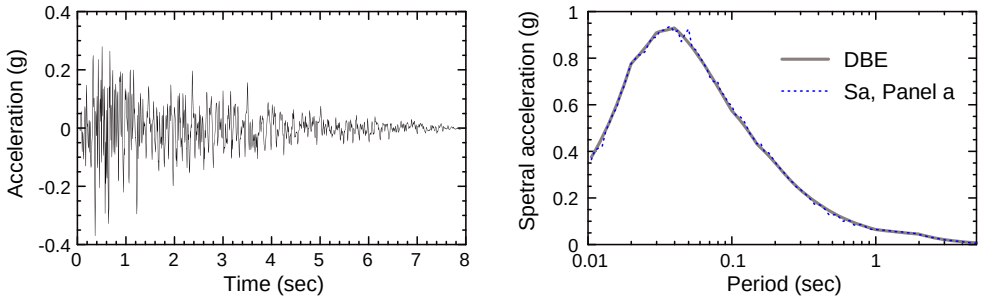

a. time series (horizontal component 1) b. spectral acceleration (horizontal component 1)

Figure 5. Sample DBE-SC acceleration time series and the corresponding 5% damped response spectra for the North Anna site.

Because the number of strong ground-motion records in CEUS is limited, synthetic ground motions were developed in two steps. Step 1 involved the use of the deaggregtion data for the North Anna site and the computer code 'Strong Ground Motion Simulation' [20] to generate CEUS-type seed ground motions, which were then spectrally matched to the DBE spectra of Figure 4 in step 2 using the computer code RSPMATCH [21].

The SGMS code is based on the Specific Barrier Model, which provides a complete and self-consistent description of the heterogeneous earthquake faulting process and can capture the rich high-frequency content in CEUS ground motions [22]. The RSPMATCH code adjusts the spectral ordinates of the seed motions by adding wavelets to the acceleration time series in the time domain.

Thirty sets of DBE-SC ground motions were developed and each set of ground motions included two horizontal components and a vertical component. Panel (a) of Figure 5 presents a sample DBE-SC acceleration time series and panel (b) presents the target and achieved spectral accelerations for the time series of panel (a). The spectral accelerations for the time series of panel a closely match the target. Panel (a) of Figure 6 presents the spectral accelerations for horizontal component 1 of all 30 sets of DBE-SC ground motions. Each spectrum of Figure 6 (a) closely matches the target.

3.1.3. Maximum-minimum spectra compatible ground motions. A second set of 30 pairs of ground motions, MM-SC ground motions, were developed by amplitude scaling the 30 sets of DBE-SC ground motions to represent the maximum spectral demand and the demand at the orientation perpendicular to the maximum direction, termed the *minimum* demand. The maximum spectral demand at a given period was defined as the maximum of the spectral accelerations at orientations between 0° to 180° for a pair (the two orthogonal horizontal components) of ground motions [23].

For each set of DBE-SC motions, the two horizontal components were amplitude scaled by F_{H_i} and $1/F_{H_i}$, respectively, and the vertical component was amplitude scaled by F_{V_i}. Note that the geometric-mean spectrum for the two scaled horizontal components of a set of ground motions is still similar to the horizontal DBE spectrum of Figure 4. The factors F_{H_i} (F_{V_i}) with $i = 1, 30$ were determined using a lognormal distribution with the median of 1.3 (1.0) and logarithmic standard deviation of 0.13 (0.18) using the Latin Hypercube Sampling procedure. Panel (b) of Figure 6 presents the spectral accelerations for the horizontal component 1 (i.e., the maximum component) of all 30 sets of MM-SC ground motions.

The distribution of F_{H_i} was based on the study of Huang *et al.* [23], where the median ratio of maximum to geometric-mean (hereafter termed geomean[2]) spectral demands was shown to vary between 1.2 and 1.4 and the logarithmic standard deviation of the ratio varied between 0.11 and 0.13 at periods greater than 2 s.

[2]The geomean demand at a given period is computed as the square root of the product of the spectral demands for two orthogonal horizontal ground-motion components.

DOI: 10.1002/eqe

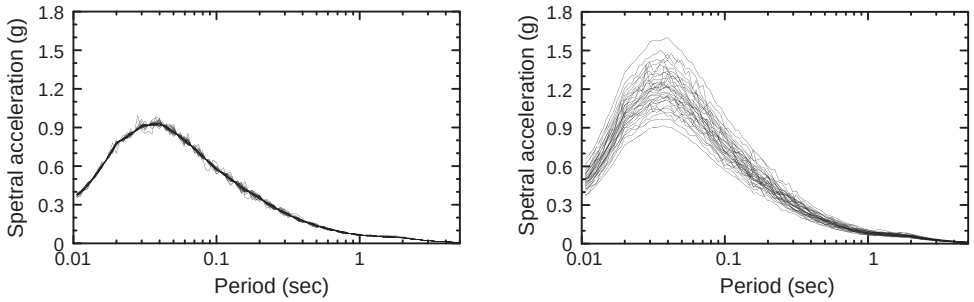

a. spectral acceleration (DBE-SC, horizontal component 1)

b. spectral acceleration (MM-SC, maximum component)

Figure 6. Five-percent damped response spectra for the DBE-SC and MM-SC ground-motion bins for the North Anna site.

3.2. Analysis sets

SAP2000 Nonlinear (CSI 2007) was used to perform the response-history analysis of the models of base-isolated NPPs. Each model was composed of a rigid mass supported by a link element representing the isolation system. Each model had three degrees of freedom: two horizontal and one vertical. Only the results for the LR and FP models with $Q_d = 0.03W$ and the three LDR models described in Section 2.1 are presented herein for the sample CEUS rock site. Two percent inherent damping was assigned to each mode included in the response-history analysis.

Response-history analysis was performed for two intensities of shaking: (1) 100% DBE shaking, using the 60 sets of DBE-SC and MM-SC ground motions, and (b) 150% DBE shaking, using the DBE-SC and MM-SC ground motions but with the amplitude of the acceleration time series multiplied by 1.5. At each intensity level, four sets of analyses were performed for each of the best-estimate models for this study and the corresponding property-varied models. Table II summarizes the four analysis sets used in this study, denoted G0, M0, M1, and M2.

Set G0 involves response-history analysis of a best-estimate model subjected to 100% and 150% of the 30 sets of DBE-SC ground motions and produces 30 realizations for each of peak bearing displacement and shearing force in the horizontal plane. Here, the letter G stands for geomean beause the target horizontal DBE spectrum of Figure 4 is a geomean of two horizontal components and the number 0 is used to denote analysis performed using best-estimate models. The data developed from analysis of Set G0 is used to benchmark all other results.

Set M0 is similar to Set G0 but uses 100% and 150% of the 30 sets of MM-SC ground motions. For Set M1 (M2), each of the 30 models associated with a given best-estimate model and mechanical-property scale factors of Bin F1 (F2) is analyzed using the 100% and 150% of 30 sets of MM-SC ground motions. At a given intensity, sets M1 and M2 each produce 900 realizations (30 sets of ground motions $\times$ 30 models) for peak horizontal bearing displacement and transmitted shearing force.

Table II. Analysis sets for this study.

Set	Ground motions		Number of models	Quality control on isolators	Number of realizations for responses
	Intensity	Bin			
G0	100%, 150%	DBE-SC	1	N/A	30
M0	100%, 150%	MM-SC	1	N/A	30
M1	100%, 150%	MM-SC	30	excellent	900
M2	100%, 150%	MM-SC	30	good	900

DOI: 10.1002/eqe

3.3. Analysis results for the sample rock site in CEUS

3.3.1. Peak displacement and shearing force. **All realizations in an analysis set are assumed to distribute lognormally with median (θ) and logarithmic standard deviation (b) computed using the following equations:**

$$\theta = \exp\left(\frac{1}{n}\sum_{i=1}^{n} \ln y_i\right) \tag{2}$$

$$b = \sqrt{\frac{1}{n-1}\sum_{i=1}^{n} (\ln y_i - \ln \theta)^2} \tag{3}$$

where n is the total number of the realizations (peak displacement or force response) in an analysis set: 30 for sets G0 and M0, and 900 for sets M1 and M2. Variable y_i is the ith realization in an analysis set.

Table III presents θ and b of peak displacement and transmitted shearing force for each case, (realistic) model and shaking intensity analyzed in this study. The key observations are presented below. We note that the displacements in the LR and FP systems are very small and that the observations presented below may not apply to cases where the shaking intensity is significantly greater than that of Figure 4.

1. **For a given model and shaking intensity, the values of θ for M0, M1, and M2 are identical or nearly identical. The median response for analyses accounting for variability in the mechanical properties of the isolation system (i.e., M1 and M2) can be estimated without bias using analysis of a best-estimate model (i.e. M0).**
2. **For LR and FP systems, the ratio of θ for M0 to G0 for displacement ranges between 1.1 and 1.2 and that for shearing force ranges between 1.0 and 1.1; for LDR systems, the ratios for both displacement and shearing force are about 1.15. If analysis is performed using DBE-SC ground motions (i.e., Set G0), the median displacement should be increased by 15% to 20% and the median shearing force should be increased by 10% to address variability in spectral demands for rock sites in CEUS.**

Table III. Medians (θ) and dispersions (b) of peak displacement and shearing force for the North Anna site.

Model	100% DBE								150% DBE							
	θ (mm or %W)				b				θ (mm or %W)				b			
	G0	M0	M1	M2	G0	M0	M1	M2	G0	M0	M1	M2	G0	M0	M1	M2
Displacement																
LR_T2Q3	31	35	35	35	0.10	0.12	0.12	0.13	43	50	50	50	0.13	0.13	0.14	0.14
LR_T3Q3	35	40	40	40	0.11	0.13	0.13	0.14	50	58	58	58	0.13	0.17	0.17	0.18
LR_T4Q3	37	43	43	43	0.11	0.14	0.15	0.15	52	63	63	62	0.12	0.17	0.17	0.17
FP_T2Q3	9.4	11	11	11	0.18	0.25	0.24	0.25	18	23	23	23	0.19	0.23	0.23	0.25
FP_T3Q3	10	12	12	12	0.20	0.24	0.24	0.24	19	24	24	24	0.20	0.23	0.23	0.24
FP_T4Q3	11	13	13	13	0.21	0.23	0.23	0.24	20	25	25	25	0.21	0.23	0.23	0.25
LDR_T2	61	70	70	69	0.12	0.10	0.10	0.10	92	105	105	104	0.12	0.10	0.10	0.10
LDR_T3	63	72	72	72	0.11	0.10	0.10	0.10	94	109	109	108	0.11	0.10	0.10	0.10
LDR_T4	63	73	73	73	0.12	0.12	0.12	0.12	95	110	110	110	0.12	0.12	0.12	0.12
Shearing force																
LR_T2Q3	5.7	6.3	6.3	6.3	0.07	0.08	0.09	0.09	7.2	8.0	8.0	8.0	0.09	0.09	0.09	0.10
LR_T3Q3	4.3	4.6	4.6	4.6	0.06	0.06	0.07	0.08	5.1	5.6	5.6	5.6	0.06	0.09	0.09	0.09
LR_T4Q3	3.7	4.0	4.0	4.0	0.04	0.05	0.06	0.08	4.2	4.5	4.5	4.5	0.04	0.06	0.07	0.10
FP_T2Q3	4.2	4.3	4.3	4.3	0.07	0.09	0.09	0.11	5.3	5.6	5.6	5.6	0.09	0.14	0.14	0.14
FP_T3Q3	3.8	3.9	3.9	3.9	0.06	0.06	0.07	0.10	4.5	4.6	4.6	4.6	0.07	0.09	0.10	0.12
FP_T4Q3	3.7	3.7	3.7	3.7	0.05	0.06	0.07	0.10	4.3	4.3	4.3	4.3	0.06	0.08	0.09	0.12
LDR_T2	6.2	7.1	7.0	7.0	0.12	0.10	0.10	0.12	9.3	10.6	10.5	10.4	0.12	0.10	0.10	0.12
LDR_T3	2.8	3.2	3.2	3.2	0.11	0.10	0.11	0.14	4.2	4.9	4.9	4.8	0.11	0.10	0.11	0.14
LDR_T4	1.6	1.8	1.8	1.8	0.12	0.12	0.13	0.16	2.4	2.8	2.8	2.7	0.12	0.12	0.13	0.16

DOI: 10.1002/eqe

(3) For LR (FP) systems, the ratio of θ at 150% to 100% DBE shaking for a given model and analysis set (e.g., the θ for LR_T2Q3 and G0 for 150% DBE shaking divided by that for 100% DBE shaking) ranges between 1.4 (1.7) and 1.5 (2.0) for displacement and between 1.1 (1.1) and 1.3 (1.3) for shearing force; for LDR systems, the ratio for both displacement and shearing force are about 1.5. Such ratios could be used to estimate median and other fractile isolator responses for rock sites in CEUS in the absence of computations for 150% DBE shaking.

(4) The dispersions (b) in displacement are higher than those in transmitted shearing force. For displacement, the dispersion increases if the variability in the spectral demand is included in the analysis and does not further increase (or increase insignificantly) as the variability in the bearing properties is considered. For transmitted shearing force, although there are significant percentage differences in the dispersions between sets G0 and M2, all values of b are small.

3.3.2. Number of ground motions for analysis. The number of sets of ground motions required to achieve a reliable estimate of median response depends on the dispersion in the response and the required precision and confidence level for the estimate. For a lognormal distribution with a median of θ and a logarithmic standard deviation of b, the number of realizations (n) required to estimate the median within a range of $\theta(1 \pm X)$ with Z% of confidence can be computed as [24]

$$n = \left(\frac{\Phi^{-1}\left(1 - \frac{a}{2}\right) \cdot b}{\ln(1 + X)} \right)^2 \tag{4}$$

where Φ^{-1} is the inverse standardized normal distribution function and $a = 1 - Z$%.

The dispersion in the peak response ranges between 0.1 and 0.25 per Table III. For b = 0.1 (0.25), the minimum number of sets of ground motions per (4) to ensure a 90% confidence of the true median displacement being within $\pm$10% of the estimated value is 3 (19).

3.3.3. Response scale factors for design. To develop procedures for the analysis and design of base isolation systems satisfying the dual performance objectives presented in ASCE 43-05, we compute factors to scale the median responses for sets G0 and M0 and 100% DBE shaking to the responses corresponding to (1) 1% probability of exceedance (PE) for sets M1 and M2 for 100% DBE shaking and (2) 10% PE for sets M1 and M2 for 150% DBE shaking. The factors for isolation-system displacement and transmitted shearing force for rock sites in CEUS are presented in Tables IV and V, respectively.

If response-history analysis is performed using only the DBE-SC ground motions, the factors in the second through fifth columns of Tables IV and V can be used to address the influence of both maximum-demand orientation and the variation in the material properties of isolation systems on responses. The factor for displacement (force) corresponding to 1% PE at 100% DBE shaking ranges between 1.4 (1.2) and 2.2 (1.7) and that corresponding to 10% PE at 150% DBE shaking ranges between 1.9 (1.3) and 3.4 (2.1) for all models of Table IV.

Table IV. Ratios of displacement for 1% (10%) exceedance probability at 100% (150%) DBE to $\theta_{G0,\,DBE}$ and $\theta_{M0,\,DBE}$ for the North Anna site.

Model	$\frac{D_{M1;DBE;99th}}{\theta_{G0;DBE}}$	$\frac{D_{M1;150\%DBE;90th}}{\theta_{G0;DBE}}$	$\frac{D_{M2;DBE;99th}}{\theta_{G0;DBE}}$	$\frac{D_{M2;150\%DBE;90th}}{\theta_{G0;DBE}}$	$\frac{D_{M1;DBE;99th}}{\theta_{M0;DBE}}$	$\frac{D_{M1;150\%DBE;90th}}{\theta_{M0;DBE}}$	$\frac{D_{M2;DBE;99th}}{\theta_{M0;DBE}}$	$\frac{D_{M2;150\%DBE;90th}}{\theta_{M0;DBE}}$
LR_T2Q3	1.54	1.96	1.55	1.98	1.34	1.70	1.35	1.72
LR_T3Q3	1.56	2.09	1.59	2.10	1.36	1.83	1.40	1.84
LR_T4Q3	1.64	2.09	1.66	2.09	1.40	1.79	1.42	1.78
FP_T2Q3	2.13	3.28	2.18	3.35	1.77	2.72	1.81	2.78
FP_T3Q3	2.12	3.25	2.17	3.31	1.73	2.65	1.77	2.71
FP_T4Q3	2.09	3.20	2.14	3.26	1.71	2.62	1.75	2.67
LDR_T2	1.43	1.94	1.44	1.94	1.25	1.70	1.26	1.70
LDR_T3	1.46	1.97	1.47	1.98	1.26	1.70	1.27	1.71
LDR_T4	1.52	2.02	1.52	2.02	1.31	1.74	1.31	1.74

DOI: 10.1002/eqe

Table V. Ratios of shearing force for 1% (10%) exceedance probability at 100% (150%) DBE to $\theta_{G0,DBE}$ and $\theta_{M0,DBE}$ for the North Anna site.

Model	$\frac{F_{M1;DBE;99th}}{\theta_{G0;DBE}}$	$\frac{F_{M1;150\%DBE;90th}}{\theta_{G0;DBE}}$	$\frac{F_{M2;DBE;99th}}{\theta_{G0;DBE}}$	$\frac{F_{M2;150\%DBE;90th}}{\theta_{G0;DBE}}$	$\frac{F_{M1;DBE;99th}}{\theta_{M0;DBE}}$	$\frac{F_{M1;150\%DBE;90th}}{\theta_{M0;DBE}}$	$\frac{F_{M2;DBE;99th}}{\theta_{M0;DBE}}$	$\frac{F_{M2;150\%DBE;90th}}{\theta_{M0;DBE}}$
LR_T2Q3	1.35	1.56	1.36	1.58	1.22	1.42	1.24	1.44
LR_T3Q3	1.25	1.43	1.28	1.44	1.17	1.34	1.20	1.35
LR_T4Q3	1.22	1.33	1.29	1.36	1.15	1.25	1.21	1.28
FP_T2Q3	1.30	1.61	1.35	1.62	1.24	1.54	1.29	1.55
FP_T3Q3	1.21	1.39	1.29	1.42	1.19	1.36	1.26	1.39
FP_T4Q3	1.19	1.32	1.28	1.37	1.18	1.31	1.27	1.35
LDR_T2	1.44	1.94	1.48	1.96	1.26	1.70	1.30	1.72
LDR_T3	1.50	2.00	1.61	2.08	1.29	1.72	1.39	1.79
LDR_T4	1.56	2.05	1.67	2.12	1.34	1.76	1.44	1.83

If response-history analysis is performed using the MM-SC ground motions, the factors in the sixth through ninth columns of Table IV and Figure 4 can be used to address the impact of variation in isolator material properties on response. The factor for displacement (force) corresponding to 1% PE at 100% DBE shaking ranges between 1.3 (1.2) and 1.8 (1.4) and that corresponding to 10% PE at 150% DBE shaking ranges between 1.7 (1.3) and 2.8 (1.8) for all models of Table V. On the basis of the data of Tables IV and V, the design of base isolation systems is always governed by the case for 10% PE at 150% DBE shaking.

The ratios of Table IV for FP isolation systems are higher than the other two types of isolation systems because (1) the conventional single-concave FP systems have higher pre-yield stiffness than that of the LR systems and the elastic stiffness of the LDR systems and (2) the isolation displacements for the cases of Table IV are small. The use of the triple concave FP bearing will increase the yield displacement to a value similar to that adopted for the LR models [15] and will likely reduce the ratios of Table IV for the FP isolation systems.

4. STUDIES FOR A SOIL SITE IN CEUS

4.1. Ground motions and analysis sets

The site of the Vogtle NPP in Waynesboro, GA is a representative soil site for NPPs in CEUS. The horizontal and vertical DBE spectra used in this study for the Vogtle site are presented in Figure 7. The horizontal spectrum of Figure 7 is a uniform-risk spectrum corresponding to a MAFE of 10^{-5} developed by the Southern Nuclear Operating Company for the Vogtle Early Site Permit Application [25]. The horizontal DBE spectrum of Figure 7 was scaled by the V/H factors of 0.9 at periods smaller than 0.07 s (15 Hz) and 0.5 at periods greater than 1 s. Interpolation was used to determine the scale

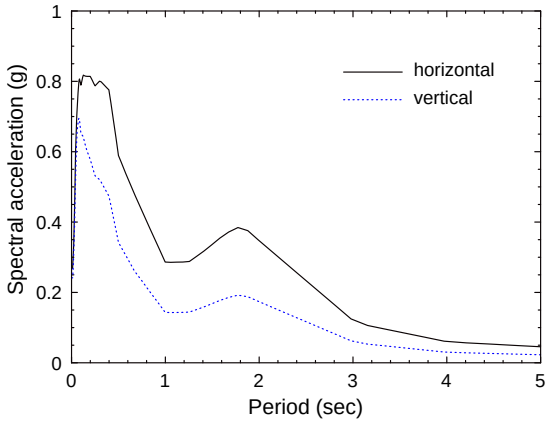

Figure 7. Horizontal and vertical 5% damped DBE spectra for the Votgle NPP site.

DOI: 10.1002/eqe

factors at periods between 0.07 and 1 s. The technical basis for the V/H scale factors for the spectra of Figure 7 is provided in [24].

The procedures of Section 3.1 were used to develop 30 sets of DBE-SC and MM-SC ground motions for the DBE shaking of Figure 7. The analysis sets of Table II, namely, sets G0, M0, M1 and M2, were repeated using the LR and FP models described in Section 2 and the ground motions generated for the Vogtle site. Only the results for the models with Q_d/W equal to 3% and 6% and T_d equal to 3 and 4 s are presented herein. The models with T_d equal to 2 s are considered inappropriate for the spectral shape of Figure 7, where a local peak is evident at a period close to 2 s.

4.2. Analysis results for the sample soil site in CEUS

4.2.1. Peak displacement and shearing force. Table VI presents θ and b of peak displacement and transmitted shearing force for each case, (realistic) model and shaking intensity analyzed for the Votgle site. The key observations are presented below:

(1) The ratios of θ for M1/M0 and M2/M1 are either equal to or very close to 1 for all models and shaking intensities of Table VI. The median response for analyses accounting for the variability in isolation-system material properties (i.e., sets M1 and M2) can be estimated without bias using analysis of a best-estimate model (i.e., Set M0).
(2) The ratios of θ for M0/G0 for displacement range between 1.2 and 1.3 (except for FP_T3Q6 and 100% DBE shaking, for which the ratio is 1.36; however, the ratio drops to 1.27 for 150% DBE shaking) and those for shearing force range between 1.1 and 1.2. If analysis is performed using geomean-spectrum-compatible ground motions, the median displacement should be increased by 20% to 30% and the median shearing force should be increased by 20% to address variability in spectral demands.
(3) The ratio of θ at 150% to 100% DBE shaking for LP systems ranges between 1.5 and 1.8 for bearing displacement and between 1.2 and 1.5 for shearing force. For a given model, the ratio for displacement is higher than that for shearing force: an expected result considering the bilinear hysteresis behavior for the isolation systems. At a given T_d, the ratio of θ for bearing displacement increases as Q_d increases. The results for FP systems show similar trends as those for LP systems.
(4) The dispersion in bearing displacement is generally higher than or similar to that for shearing force. The percentage increase in b because of the variability in spectral demand is higher than that because of the variability in the mechanical properties of the isolation system.[3]
(5) If we assume that the response-history analysis is performed for Set G0 and the dispersions in the peak bearing displacement for 100% (150%) DBE shaking are smaller than 0.21 (0.18) per Table VI, the minimum number of pairs of ground motions per (4) to ensure a 90% confidence of the true median displacement being within $\pm$10% of the estimated value is 13 (10).

4.2.2. Response scale factors for design. The analyses of Tables IV and V were repeated for the Votgle site and results are presented in Tables VII and VIII, respectively. Similar to the trend observed in Tables IV and V for the North Anna site, the design of base isolation systems is always governed by the case for 10% PE at 150% DBE shaking.

If response-history analysis for the design of isolation systems is performed using only the DBE-SC ground motions, the scale factor for displacement (shearing force) corresponding to 10% PE at 150% DBE shaking ranges between 2.34 (1.72) and 2.93 (2.32) for LR models and between 2.57 (2.07) and 3.85 (2.81) for FP models.

[3]For a given model at a given ground-motion intensity, the value of b of Table VI for Set G0 is 25%–65% smaller than that for sets M0, M1, and M2 for bearing displacement; the difference in b between sets M0, M1, and M2 for bearing displacement is relatively smaller.

DOI: 10.1002/eqe

Table VI. Medians (θ) and dispersions (b) of peak displacement and shearing force for the analysis sets of Table for the Votgle site.

	100% DBE								150% DBE							
	θ (mm or %W)				b				θ (mm or %W)				b			
Model	G0	M0	M1	M2	G0	M0	M1	M2	G0	M0	M1	M2	G0	M0	M1	M2
								Displacement								
LR_T3Q3	289	349	348	347	0.13	0.18	0.18	0.19	467	558	557	555	0.12	0.15	0.15	0.16
LR_T3Q6	204	264	263	263	0.16	0.24	0.23	0.24	368	456	455	454	0.15	0.21	0.21	0.22
LR_T4Q3	227	274	274	274	0.13	0.20	0.20	0.20	352	425	426	427	0.11	0.18	0.18	0.18
LR_T4Q6	195	238	238	238	0.15	0.23	0.23	0.23	309	373	374	374	0.16	0.23	0.23	0.23
FP_T3Q3	246	303	303	303	0.14	0.20	0.19	0.20	433	523	523	523	0.12	0.15	0.15	0.15
FP_T3Q6	140	190	190	189	0.21	0.30	0.30	0.31	308	391	391	391	0.18	0.25	0.24	0.25
FP_T4Q3	193	240	240	240	0.15	0.22	0.22	0.22	325	403	403	403	0.12	0.19	0.19	0.19
FP_T4Q6	128	168	168	168	0.20	0.29	0.28	0.29	255	319	319	319	0.18	0.26	0.25	0.26
								Shearing force								
LR_T3Q3	15.3	18.1	18.1	18.0	0.11	0.16	0.17	0.21	23.0	27.3	27.2	27.1	0.11	0.15	0.16	0.21
LR_T3Q6	14.6	17.5	17.5	17.4	0.10	0.16	0.16	0.17	21.5	25.6	25.6	25.5	0.11	0.18	0.18	0.20
LR_T4Q3	8.4	9.6	9.6	9.6	0.09	0.15	0.16	0.18	11.3	13.3	13.3	13.3	0.09	0.16	0.16	0.18
LR_T4Q6	10.6	11.8	11.8	11.7	0.07	0.12	0.12	0.13	13.1	15.0	15.0	15.0	0.10	0.15	0.15	0.16
FP_T3Q3	14.8	17.9	17.9	17.9	0.13	0.21	0.21	0.21	25.6	30.6	30.6	30.6	0.12	0.18	0.18	0.18
FP_T3Q6	12.7	15.4	15.4	15.4	0.11	0.19	0.19	0.19	22.0	26.4	26.5	26.5	0.13	0.24	0.24	0.23
FP_T4Q3	8.4	9.8	9.8	9.8	0.11	0.17	0.17	0.17	12.6	15.0	15.0	15.0	0.12	0.17	0.17	0.17
FP_T4Q6	9.9	11.1	11.1	11.1	0.07	0.14	0.14	0.14	14.2	16.4	16.4	16.4	0.11	0.18	0.18	0.18

Table VII. Ratios of displacement for 1% (10%) exceedance probability at 100% (150%) DBE to $\theta_{G0,DBE}$ and $\theta_{M0,DBE}$ for the analysis sets of Table for the Votgle site.

Model	$\frac{D_{M1;DBE;99th}}{\theta_{G0;DBE}}$	$\frac{D_{M1;150\%DBE;90th}}{\theta_{G0;DBE}}$	$\frac{D_{M2;DBE;99th}}{\theta_{G0;DBE}}$	$\frac{D_{M2;150\%DBE;90th}}{\theta_{G0;DBE}}$	$\frac{D_{M1;DBE;99th}}{\theta_{M0;DBE}}$	$\frac{D_{M1;150\%DBE;90th}}{\theta_{M0;DBE}}$	$\frac{D_{M2;DBE;99th}}{\theta_{M0;DBE}}$	$\frac{D_{M2;150\%DBE;90th}}{\theta_{M0;DBE}}$
LR_T3Q3	1.83	2.34	1.85	2.37	1.51	1.94	1.53	1.96
LR_T3Q6	2.22	2.91	2.24	2.93	1.72	2.26	1.73	2.27
LR_T4Q3	1.92	2.36	1.93	2.37	1.60	1.96	1.60	1.96
LR_T4Q6	2.06	2.58	2.07	2.58	1.69	2.11	1.69	2.11
FP_T3Q3	1.93	2.57	1.95	2.58	1.57	2.09	1.58	2.09
FP_T3Q6	2.72	3.83	2.80	3.85	2.00	2.82	2.06	2.83
FP_T4Q3	2.09	2.65	2.10	2.66	1.68	2.13	1.68	2.13
FP_T4Q6	2.52	3.44	2.56	3.45	1.93	2.63	1.96	2.64

Table VIII. Ratios of shearing force for 1% (10%) exceedance probability at 100% (150%) DBE to $\theta_{G0,DBE}$ and $\theta_{M0,DBE}$ for the analysis sets of Table for the Votgle site.

Model	$\frac{F_{M1;DBE;99th}}{\theta_{G0;DBE}}$	$\frac{F_{M1;150\%DBE;90th}}{\theta_{G0;DBE}}$	$\frac{F_{M2;DBE;99th}}{\theta_{G0;DBE}}$	$\frac{F_{M2;150\%DBE;90th}}{\theta_{G0;DBE}}$	$\frac{F_{M1;DBE;99th}}{\theta_{M0;DBE}}$	$\frac{F_{M1;150\%DBE;90th}}{\theta_{M0;DBE}}$	$\frac{F_{M2;DBE;99th}}{\theta_{M0;DBE}}$	$\frac{F_{M2;150\%DBE;90th}}{\theta_{M0;DBE}}$
LR_T3Q3	1.78	2.20	1.91	2.32	1.50	1.85	1.61	1.95
LR_T3Q6	1.76	2.22	1.80	2.27	1.47	1.85	1.50	1.90
LR_T4Q3	1.67	1.96	1.74	2.01	1.45	1.70	1.51	1.75
LR_T4Q6	1.47	1.72	1.51	1.74	1.32	1.55	1.36	1.57
FP_T3Q3	1.97	2.61	1.97	2.61	1.63	2.16	1.63	2.16
FP_T3Q6	1.89	2.81	1.89	2.81	1.56	2.33	1.56	2.33
FP_T4Q3	1.74	2.23	1.74	2.23	1.48	1.91	1.48	1.91
FP_T4Q6	1.55	2.07	1.55	2.07	1.39	1.85	1.39	1.85

If response-history analysis is performed using the MM-SC ground motions, the factor for displacement (force) corresponding to 10% PE at 150% DBE shaking ranges between 1.94 (1.55) and 2.27 (1.95) for LR models and between 2.09 (1.85) and 2.83 (2.33) for FP models.

DOI: 10.1002/eqe

5. STUDIES FOR A ROCK SITE IN WUS

5.1. Ground motions and analysis sets

The site of the Diablo Canyon nuclear power plant in San Luis Obispo County, CA, is a representative rock site for an NPP in WUS. The horizontal and vertical DBE spectra for the Diablo Canyon study are presented in Figure 8 and was developed based on the information provided by staff at the United States Nuclear Regulatory Commission (USNRC). More information on the generation of Figure 8 is presented in [19].

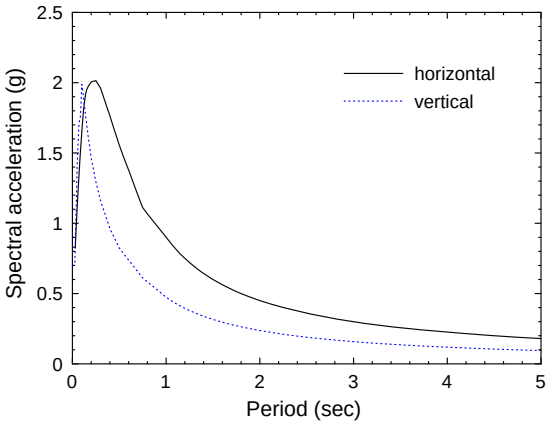

Figure 8. Horizontal and vertical 5% damped DBE spectra for the Diablo Canyon NPP site.

Table IX. Seed ground motions for the Diablo Canyon study.

No.	Event	Station	Date	M_w	r (km)	V_{S30} (m/s)
1	San Fernando	Lake Hughes #4	1971/02/09	6.61	25.1	821.7
2	San Fernando	Pacoima Dam (upper left)	1971/02/09	6.61	1.8	2016.1
3	San Fernando	Pasadena	1971/02/09	6.61	21.5	969.1
4	Tabas, Iran	Tabas	1978/09/16	7.35	2.1	766.8
5	Irpinia, Italy	Auletta	1980/11/23	6.90	9.6	1000.0
6	Irpinia, Italy	Bagnoli Irpinio	1980/11/23	6.90	8.2	1000.0
7	Irpinia, Italy	Bisaccia	1980/11/23	6.90	21.3	1000.0
8	Irpinia, Italy	Sturno	1980/11/23	6.90	10.8	1000.0
9	Loma Prieta	Gilroy - Gavilan Coll.	1989/10/18	6.93	10.0	729.7
10	Loma Prieta	Gilroy Array #1	1989/10/18	6.93	9.6	1428.0
11	Loma Prieta	UCSC	1989/10/18	6.93	18.5	714.0
12	Loma Prieta	UCSC Lick Observatory	1989/10/18	6.93	18.4	714.0
13	Cape Mendocino	Petrolia	1992/04/25	7.01	8.2	712.8
14	Northridge	Burbank - Howard Rd.	1994/01/17	6.69	16.9	821.7
15	Northridge	Chalon Rd	1994/01/17	6.69	20.5	740.1
16	Northridge	Griffith Park Observatory	1994/01/17	6.69	23.8	1015.9
17	Northridge	Wonderland Ave	1994/01/17	6.69	20.3	1222.5
18	Northridge	LA 00	1994/01/17	6.69	19.1	706.2
19	Northridge	Lake Hughes #4	1994/01/17	6.69	31.7	821.7
20	Northridge	Pacoima Dam (downstr)	1994/01/17	6.69	7.0	2016.1
21	Northridge	Pacoima Dam (upper left)	1994/01/17	6.69	7.0	2016.1
22	Northridge	Santa Susana Ground	1994/01/17	6.69	16.7	715.1
23	Northridge	Vasquez Rocks Park	1994/01/17	6.69	23.6	996.4
24	Kocaeli, Turkey	Gebze	1999/08/17	7.51	10.9	792.0
25	Kocaeli, Turkey	Izmit	1999/08/17	7.51	7.2	811.0
26	Chi-Chi, Taiwan	TCU045	1999/09/20	7.62	26.0	704.6
27	Chi-Chi, Taiwan	TCU102	1999/09/20	7.62	1.5	714.3
28	Duzce, Turkey	Lamont 1060	1999/11/12	7.14	25.9	782.0
29	Manjil, Iran	Abbar	1990/06/20	7.37	12.6	724.0
30	Loma Prieta	Los Gatos - Lexington Dam	1989/10/18	6.93	5.0	1070.3

DOI: 10.1002/eqe

The deaggregation of the seismic hazard at periods of 2 and 3 s and an annual frequency of exceedance of 10^{-4} for the Diablo Canyon NPP site was generated using United States Geological Survey (USGS) interactive deaggregation tool [26]. The moment magnitude (M_w) and distance (r) for the modal and mean events range between 7.5 and 7.8 (M_w) and 10 and 20 km (r).

The seed ground motions used to develop the DBE spectrum-compatible ground motions for the Diablo Canyon study were selected from the PEER NGA Database [27]. The number of rock-site records in the PEER NGA Database within the ranges of M_w and r identified above is less than 30. To select 30 sets of seed ground motions, we expanded the range to M_w greater than 6.6, r less than 32 km and V_{S30} (the average shear-wave velocity to 30-m depth) greater than 700 m/s. Table IX presents the 30 sets of seed ground motions used for the Diablo Canyon study.

Each set of the seed ground motions of Table IX was spectrally matched to the DBE spectra of Figure 8 using the computer code RSPMATCH [21]. The 30 sets of DBE-SC ground motions were amplitude scaled to develop the MM-SC ground motions using the scaling procedure described in Section 3.1. The analysis sets of Table II were repeated using the LR and FP models described in Section 2 and the ground motions generated for the Diablo Canyon site. Only the results for the 12 models identified in the first column of Table X are presented herein. The other models have displacements associated with 10% PE and 150% DBE shaking in the analysis set M2 greater than 1500 mm and are not presented because better isolation systems could be used.

The amplitude of the spectral response in the vertical direction for 100% DBE (and 150% DBE) shaking is such that separation of the containment vessel from the foundation is possible in either conventional or isolated configurations. Although disengagement of the containment vessel from the foundation could be accommodated, alternate analysis tools and numerical models from those described in Section 2.1 would be required for response computations. Analysis codes and component models would have addressed disengagement and recontact for conventional and FP-isolated containment vessels and differences in compressive and tensile isolator axial stiffness for LR-isolated containment vessels.

Numerical and experimental studies have shown that vertical earthquake shaking does not substantially affect the displacement response of either elastomeric or sliding isolation systems [28–31]. Given that the numerical tools of Section 2.1 may not reliably capture the effects of the intense vertical shaking expected at the Diablo Canyon site for 100% and 150% DBE shaking, the discussion that follows focuses solely on displacements of the isolation systems.

Table X. Medians (θ) and dispersions (b) of peak displacement for the analysis sets of Table for the Diablo Canyon site.

Model	100% DBE								150% DBE							
	θ (mm)				b				θ (mm)				b			
	G0	M0	M1	M2	G0	M0	M1	M2	G0	M0	M1	M2	G0	M0	M1	M2
LR_T2Q3	488	572	573	576	0.10	0.13	0.13	0.14	792	932	932	936	0.09	0.12	0.12	0.13
LR_T2Q6	401	473	473	472	0.14	0.20	0.20	0.21	678	797	797	798	0.12	0.16	0.16	0.17
LR_T2Q9	338	404	404	405	0.19	0.25	0.25	0.25	595	703	703	702	0.14	0.21	0.21	0.21
LR_T3Q6	494	584	585	585	0.19	0.26	0.25	0.25	862	1039	1039	1041	0.18	0.22	0.22	0.22
LR_T3Q9	404	471	472	472	0.20	0.28	0.28	0.28	729	863	864	865	0.20	0.26	0.26	0.26
LR_T4Q9	418	493	493	495	0.21	0.29	0.29	0.29	779	951	951	950	0.19	0.24	0.24	0.24
FP_T2Q3	492	571	571	572	0.11	0.14	0.14	0.14	819	953	953	953	0.11	0.13	0.13	0.13
FP_T2Q6	392	461	461	461	0.15	0.22	0.21	0.22	686	800	801	801	0.13	0.17	0.17	0.17
FP_T2Q9	321	385	385	384	0.21	0.26	0.26	0.27	593	697	697	697	0.16	0.22	0.22	0.22
FP_T3Q6	471	555	556	557	0.21	0.28	0.27	0.28	852	1006	1006	1007	0.18	0.23	0.23	0.23
FP_T3Q9	374	442	443	443	0.23	0.29	0.29	0.30	707	832	833	834	0.21	0.28	0.27	0.27
FP_T4Q9	382	462	462	463	0.24	0.31	0.31	0.31	756	925	925	928	0.20	0.24	0.23	0.24

DOI: 10.1002/eqe

Table XI. Ratios of displacement for 1% (10%) exceedance probability at 100% (150%) DBE to $\theta_{G0,DBE}$ and $\theta_{M0,DBE}$ for the analysis sets of Table for the sample soil site in CEUS.

Model	$\frac{D_{M1;DBE;99th}}{\theta_{G0;DBE}}$	$\frac{D_{M1;150\%DBE;90th}}{\theta_{G0;DBE}}$	$\frac{D_{M2;DBE;99th}}{\theta_{G0;DBE}}$	$\frac{D_{M2;150\%DBE;90th}}{\theta_{G0;DBE}}$	$\frac{D_{M1;DBE;99th}}{\theta_{M0;DBE}}$	$\frac{D_{M1;150\%DBE;90th}}{\theta_{M0;DBE}}$	$\frac{D_{M2;DBE;99th}}{\theta_{M0;DBE}}$	$\frac{D_{M2;150\%DBE;90th}}{\theta_{M0;DBE}}$
LR_T2Q3	1.60	2.22	1.64	2.26	1.37	1.89	1.40	1.92
LR_T2Q6	1.88	2.44	1.91	2.47	1.59	2.07	1.62	2.09
LR_T2Q9	2.13	2.71	2.14	2.73	1.78	2.27	1.79	2.28
LR_T3Q6	2.12	2.79	2.13	2.79	1.79	2.35	1.80	2.35
LR_T3Q9	2.24	2.98	2.26	2.99	1.92	2.55	1.94	2.56
LR_T4Q9	2.31	3.08	2.33	3.11	1.96	2.61	1.97	2.64
FP_T2Q3	1.60	2.29	1.61	2.30	1.38	1.98	1.38	1.98
FP_T2Q6	1.93	2.52	1.94	2.53	1.64	2.15	1.65	2.15
FP_T2Q9	2.20	2.87	2.22	2.88	1.83	2.39	1.85	2.40
FP_T3Q6	2.23	2.86	2.24	2.87	1.89	2.43	1.90	2.43
FP_T3Q9	2.33	3.16	2.36	3.17	1.97	2.67	2.00	2.68
FP_T4Q9	2.47	3.27	2.49	3.31	2.05	2.71	2.06	2.74

5.2. Analysis results for the sample rock site in WUS

5.2.1. Peak displacement. **Table X presents θ and β of peak displacement for each case, (realistic) model and shaking intensity analyzed for the Diablo Canyon site. The key observations are presented below:**

(1) Similar to the trend observed in the data for the sample CEUS sites, the ratios of θ for M1/M0 and M2/M1 are either equal to or very close to 1 for all models and shaking intensities.
(2) The ratios of θ for M0/G0 are very close to 1.2. If analysis is performed using geomean-spectrum-compatible ground motions, the median displacement should be increased by 20% to address variability in spectral demands.
(3) The ratio of θ at 150% to 100% DBE shaking ranges between 1.6 and 1.9 for LP systems and 1.7 and 2.0 for FP systems.
(4) The percentage increase in β because of the variability in spectral demand is higher than that because of the variability in the mechanical properties of the isolation system: an observation also reported for the sample CEUS soil site.
(5) For Set G0 of Table X, the dispersion in the peak bearing displacement ranges between 0.09 and 0.24. For β= 0.09 (0.24), the minimum number of pairs of ground motions per (4) to ensure a 90% confidence of the true median displacement being within $\pm$10% of the estimated value is 3 (17).

5.2.2. Response scale factors for design. **The analyses of Table IV were repeated for the Diablo Canyon site and results are presented in Table XI. Similar to the trend observed in Table IV for the North Anna site, the design of base isolation systems is always governed by the case for 10% PE at 150% DBE shaking.**

If response-history analysis for the design of isolation systems is performed using only the DBE-SC (MM-SC) ground motions, the scale factor for displacement corresponding to 10% PE at 150% DBE shaking ranges between 2.22 (1.89) and 3.31 (2.74).

6. CONCLUSIONS

Nonlinear response-history analyses have been performed to study the impact of the variability in both earthquake ground motion and mechanical properties of isolation systems on the seismic responses of base-isolated NPPs. Three types of isolation systems were studied, including LR, single concave FP, and LDR isolation systems. The analyses were performed for representative rock and soil sites in CEUS and a rock site in WUS. Key conclusions are summarized below:

(1) The reduction in horizontal seismic force on the supported structure because of the implementation of a well-designed seismic isolation system is significant. For example, at a period of 0.1 (0.2) s, the 150% DBE spectral demand in the horizontal direction is 0.9*g* (0.5*g*) for the North Anna site and the values of θ of Table III for 150% DBE shaking are between 0.02*W* and 0.1*W*.

DOI: 10.1002/eqe

(2) For a given model, the ratio of median responses for Set M0 to Set G0 generally ranges between 1.1 and 1.3. The median responses for analyses using DBE-SC ground motions in both horizontal directions should be amplified to address the known variability in spectral demands.
(3) The ratios of median responses for Set M1 to Set M0 and those for Set M2 to Set M1 are either equal to or very close to 1 for all cases considered. The median response for analyses accounting for the variability in isolator material properties (i.e., M1 and M2) can be estimated without bias using analysis of a best-estimate model (i.e., M0).
(4) The factors to scale the median displacements for sets G0 and M0 and 100% DBE shaking to the displacements corresponding to (a) 1% PE for Sets M1 and M2 for 100% DBE shaking and (b) 10% PE for sets M1 and M2 for 150% DBE shaking were studied for the three represented sites. For a given site, type of isolator and analysis set (G0 or M0), the factor for 10% PE and 150% DBE shaking is greater than that for 1% PE and 100% DBE shaking. Analysis of isolator capacity and clearance to surrounding structure can be based on 10% PE for 150% DBE shaking. For a given site and type of isolator, the factor for Set G0 is always greater than that for Set M0 because the ratio of median displacement for Set M0 to Set G0 is always greater than 1. For Set G0, 10% PE and 150% DBE shaking, the upper bounds of the scale factor for the representative CEUS rock, CEUS soil and WUS rock sites are 3.4, 3.9, and 3.3, respectively; the lower bounds are 1.9, 2.3, and 2.2, respectively.
(5) The number of sets of ground motions required in a response-history analysis is a function of the dispersion in the response and the required precision and confidence level for the estimate. On the basis of the data presented herein, the dispersion in the peak responses generally ranges between 0.1 and 0.24; therefore, the minimum number of pairs of ground motions to ensure a 90% confidence of the true median displacement being within $\pm$10% of the estimated value varies between 3 and 17.

REFERENCES

1. Mayes RL, Button MR, Jones DM. Design issues for base isolated bridges: 1997 revised AASHTO code requirements. *Proceedings, Structural Engineering World Congress*, San Francisco, CA, 1998.
2. Naeim F, Kelly JM. *Design of seismic isolated structures: from theory to practice*. John Wiley: NY, 1999.
3. Eidinger JM, Kelly JM. Seismic isolation for nuclear power plants: technical and non-technical aspects in decision making. *Nuclear Engineering and Design* **1985**; 84**(3):383–409.**
4. Naeim F, Kelly JM. *Design of seismic isolated structures: from theory to practice*. John Wiley: NY, 1999.
5. Constantinou MC, Whittaker AS, Kalpakidis Y, Fenz DM, Warn GP. Performance of seismic isolation hardware under service and seismic loading. *MCEER-07-0012*, Multidisciplinary Center for Earthquake Engineering Research, State University of New York, Buffalo, NY, 2007.
6. Huang Y-N, Whittaker AS, Luco N. Seismic performance assessment of base-isolated safety-related nuclear structures. *Earthquake Engineering and Structural Dynamics* **2010**; 39**(13):1421–1442.**
7. Huang Y-N, Whittaker AS, Luco N. A probabilistic seismic risk assessment procedure for nuclear power plants: (I) Methodology. *Nuclear Engineering and Design* **2011a**; 241**(9):3996–4003.**
8. Huang Y-N, Whittaker AS, Luco N. A probabilistic seismic risk assessment procedure for nuclear power plants: (II) Application. *Nuclear Engineering and Design* **2011b**; 241**(9):3985–3995.**
9. American Society of Civil Engineers (ASCE). Seismic analysis of safety-related nuclear structures and commentary. *ASCE 4–98*, ASCE, Reston, VA, 2000.
10. American Society of Civil Engineers (ASCE). Seismic design criteria for structures, systems, and components in nuclear facilities. *ASCE/SEI 43–05*, ASCE, Reston, VA, 2005.
11. Constantinou MC, Tsopelas P, Kasalanati A, Wolff ED. Property modification factors for seismic isolation bearings. *MCEER-99-0012*, Multidisciplinary Center for Earthquake Engineering Research, State University of New York, Buffalo, NY, 1999.
12. American Association of State Highway and Transportation Officials (AASHTO). *Guide specification for seismic isolation design*. Washington: D.C, 1999.
13. Federal Emergency Management Agency (FEMA). NEHRP recommended provisions for seismic regulations for new buildings and other structures. *FEMA 450-1/2003 Edition (Provisions) and 450-2/2003 Edition (Commentary)*, FEMA, Washington, D.C, 2004.
14. Computers and Structures, Inc. (CSI). SAP2000 user's manual – version 11.0. Berkeley, CA, 2007.
15. Fenz DM, Constantinou MC. Mechanical behavior of multi-spherical sliding bearings. *MCEER-08-0007*, Multidisciplinary Center for Earthquake Engineering Research, State University of New York, Buffalo, NY, 2008.
16. Nowak AS, Collins KR. *Reliability of structures*. McGraw-Hill: Boston, 2000.

DOI: 10.1002/eqe

17. Dominion Nuclear North Anna, LLC. North Anna Early Site Permit Application (Revision 9). (Available from: www.nrc.gov/reactors/new-reactors/esp/north-anna.html) [Accessed on 1 March 2009]. 2006.
18. Bozorgnia Y, Campbell KW. The vertical-to-horizontal response spectral ratio and tentative procedures for developing simplified V/H and vertical design spectra. *Journal of Earthquake Engineering* 2004; 8(2):175–207.
19. Huang Y-N, Whittaker AS, Kennedy RP, Mayes RL. Assessment of base-isolated nuclear structures for design and beyond-design basis earthquake shaking. *MCEER-09-0008*, Multidisciplinary Center for Earthquake Engineering Research, State University of New York, Buffalo, NY, 2009.
20. Halldorsson B. Engineering Seismology Laboratory, State University of New York, Buffalo, NY. (Available from: civil.eng.buffalo.edu/engseislab/ products.htm) [Accessed on 1 March 2009]. 2004.
21. Abrahamson NA. Non-stationary spectral matching program RSPMATCH. PG&E, Internal Report, 1998.
22. Halldorsson B, Papageorgiou AS. Calibration of the specific barrier model to earthquakes of different tectonic regions. *Bulletin of the Seismological Society of America* 2005; 93(3):1099–1131.
23. Huang Y-N, Whittaker AS, Luco N. Maximum spectral demands in the near-fault region. *Earthquake Spectra* 2008; 24(1):319–341.
24. Huang Y-N, Whittaker AS, Luco N. Performance assessment of conventional and base-isolated nuclear power plants for earthquake and blast loadings. *MCEER-08-0019*, Multidisciplinary Center for Earthquake Engineering Research, State University of New York, Buffalo, NY, 2008.
25. Southern Nuclear Operating Company (SNOC). Vogtle Early Site Permit Application, SNOC. (Available from: http://adamswebsearch2.nrc.gov/idmws/ViewDocByAccession.asp?) AccessionNumber=ML081020073 [Accessed on 1 March 2009]. 2008.
26. U.S. Geological Survey (USGS). 2008 Interactive Deaggregations (Beta). (Available from: https://geohazards.usgs.gov/deaggint/2008/) [Accessed on 1 March 2009]. 2009.
27. Pacific Earthquake Engineering Research Center (PEER). PEER Ground Motion Database. (Available from: http://peer.berkeley.edu/peer_ground_motion_database) [Accessed on 1 February 2011]. 2011.
28. Zayas VA, Low SA, Mahin SA. The FPS earthquake resisting system: experimental report. *UCB/EERC-87/01*, Earthquake Engineering Research Center, University of California, Berkeley, CA, 1987.
29. Mosqueda G, Whittaker AS, Fenves GL. Characterization and modeling of Friction Pendulum bearings subjected to multiple components of excitation. *Journal of Structural Engineering* 2004; 130(3):433–442.
30. Morgan T. The use of innovative base isolation systems to achieve complex seismic performance objectives. *Ph.D. dissertation*, Department of Civil and Environmental Engineering, University of California, Berkeley, CA, 2007.
31. Fenz DM, Constantinou MC. Development, implementation, and verification of dynamic analysis models for multi-spherical sliding bearings. *MCEER-08-0018*, Multidisciplinary Center for Earthquake Engineering Research, State University of New York, Buffalo, NY, 2008b.

DOI: 10.1002/eqe